

Chemical freeze-out parametrization with mean field repulsive hadron resonance gas model

Sunny Kumar Singh,^{1,*} Nachiketa Sarkar,^{2,†} and Deeptak Biswas^{3,‡}

¹Indian Institute of Technology Gandhinagar, Palaj, Gujarat 382355

²School of Physical Sciences, National Institute of Science Education and Research,
An OCC of Homi Bhabha National Institute, Jatni-752050, India

³The Institute of Mathematical Sciences, a CI of Homi Bhabha National Institute, Chennai, 600113, India
(Dated: July 13, 2023)

We have examined the chemical freeze-out surface of the heavy-ion collision experiments within an interacting hadron resonance gas model. By considering repulsive interaction among hadrons in the mean-field level, we have suitably parameterized the freeze-out surface by fitting the yield data of mid-rapidity for the most central collision, for the collision energy available in AGS, RHIC (BES), and LHC programs. To suitably account for the repulsive interaction among mesons and (anti-) baryons, we have introduced phenomenological parameters K_M and K_B in the freeze-out parametrization. Although a finite value of these two parameters seem to be necessary to have an improved normalized *chi-square*, the effect on the rest of the parameters like temperature and relevant chemical potentials seem to be within the standard variance.

I. INTRODUCTION

The investigation of the phase structure of strongly-interacting matter stands as a pivotal and fundamental inquiry within the realm of ultra-relativistic heavy-ion physics. To comprehend the particle spectra observed in these experiments, statistical thermal models inspired by quantum chromodynamics (QCD) are employed. In particular, the transverse momentum (p_T) integrated rapidity spectra (namely dN/dY) are frozen onward the chemical freeze-out (CFO) boundary and helps to map the freeze-out surface on the phase diagram via the CFO parametrization with temperature (T) and baryon chemical potentials (μ_B) [1]. For the past few decades, the Hadron resonance Gas (HRG) model has been successfully describing the abundance of hadrons in collisions across a wide range of energies, from the SchwerIonen-Synchrotron (SIS) to the Large Hadron Collider (LHC) [2–7]. The success of the HRG model, coupled with the lack of reliable first-principle theories that can provide such parameterization for both high and low baryon density regions of the phase diagram have firmly established HRG as one of the most widely utilized models in this field.

The simplest version of the HRG model is the ideal HRG model (IHRG) [4, 5, 7], where attractive interactions among hadrons in a dilute hadron gas can be approximated by treating higher mass resonances as stable particles. Initially proposed within the relativistic virial expansion framework, using the S -matrix approach [8], this model allows for the calculation of various thermodynamic quantities [9]. However, the IHRG model encountered discrepancies in different thermodynamic quantities when compared to lattice QCD results [10, 11], particularly at the temperature range above the pseudo-critical

value. Additionally, an excess in the pion number density at chemical freeze-out was observed [12], indicating the need to incorporate short-range repulsive interactions between hadrons to achieve more accurate Equations of State (EoS) and realistic estimations of the chemical freeze-out boundary.

One of the frequently employed methods to model the short-range repulsion is the Excluded Volume Hadron Resonance Gas (EVHRG) model [12–17]. In this model, repulsive interactions are taken into account by incorporating an impenetrable volume surrounding the individual hadrons. Several versions of the EVHRG model have been proposed in the literature to determine the strength of short-range repulsive interactions through comparisons with lattice QCD calculations or experimental data. These include the diagonal EVHRG model [12], the cross-terms EVHRG [18, 19], the mass-dependent EVHRG [20, 21], and the Flavor-dependent EVHRG model [22]. Another phenomenological approach to include the interaction is the Van der Waals Hadron Resonance Gas (vdWHRG) model, which explicitly incorporates both repulsive and attractive interactions between baryons and anti-baryons [23–27].

The repulsive interactions between the various baryon-baryon and meson-meson can also be incorporated at the mean-field level [28–31]. The interacting part of the pressure is added along with the ideal one and modification is introduced into the statistical model by shifting the energy of each particle by an amount equal to $U(n) = Kn$ where n is the total hadron number density. One can incorporate the mean-field coefficients K_M and K_B to scale the repulsive interaction strength among the mesons and baryons respectively. Recent works [31] have augmented the mean-field coefficients K_B from lattice data of $\chi_2^B - \chi_4^B$ and $\chi_2^B - \chi_6^B$. In another investigation, suitable values of K_B and K_M were estimated by fitting lattice QCD data of bulk observables, cumulants, and the speed of sound [32].

In this study, we have focused on constraining the mean-field model at the chemical freeze-out boundary by com-

* sunny.singh@iitgn.ac.in

† nachiketa.sarkar@gmail.com

‡ deeptakb@gmail.com

paring it with experimental yields through a χ^2 minimization procedure. Previous applications of this mean-field model at freeze-out involved fixing the repulsive strength parameter K to explain the data of 200 AGeV S + Au collisions at CERN-SPS [33]. While earlier studies consistently suggested a value of $K_B = 450 \text{ MeV fm}^{-3}$, we aim to investigate the collision energy dependence of these phenomenological parameters by analyzing the rapidity spectra. Within this approach, for the first time we have obtained the collision energy dependence of mean-field coefficients by parameterizing the chemical freeze-out surface for RHIC and LHC energies.

We have organized the paper as follows. In Sec. II we give a short description of the ideal HRG and the MFHRG model. In Sec. III we discuss the method we have employed to extract the various parameters in the model. In Sec. IV our results and the discussion of our results are provided in the context of heavy ion collision experiments. We conclude by giving a summary of the present work in Sec. V.

II. FORMALISM

In the ideal hadron resonance gas model, the thermodynamic potential for each species is [15, 34]:

$$\begin{aligned} \ln Z_i^{id}(T, \mu, V) \\ = \pm \frac{Vg}{(2\pi)^3} \int d^3p \ln [1 \pm e^{-(E_i - \mu_i)/T}] \end{aligned} \quad (1)$$

Where the upper(lower) sign corresponds to fermions(bosons). Here g is the degeneracy factor and V is the volume. Considering the baryon number (B), electric charge (Q), and strangeness (S), the chemical potential (μ_i) of the i th hadron is determined by $\mu_i = Q_i\mu_Q + S_i\mu_S + B_i\mu_B$.

The grand thermodynamic potential for the total ensemble is given by:

$$\ln Z^{ideal} = \sum_i \ln Z_i^{ideal} \quad (2)$$

The number density of each species can be determined by:

$$\begin{aligned} n_i &= \frac{T}{V} \left(\frac{\partial \ln Z_i}{\partial \mu_i} \right)_{V,T} \\ &= \frac{g_i}{(2\pi)^3} \int \frac{d^3p}{\exp[(E_i - \mu_i)/T] \pm 1}. \end{aligned} \quad (3)$$

One can relate the thermal abundance of the detected particles at the chemical freeze-out surface with the corresponding rapidity densities as follows:

$$\left. \frac{dN_i}{dy} \right|_{\text{Det}} \simeq \left. \frac{dV}{dy} n_i^{\text{Tot}} \right|_{\text{Det}} \quad (4)$$

The total number density of each species considering decays from higher resonances can be computed as follows:

$$\begin{aligned} n_i^{\text{Tot}} &= n_i(T, \mu_B, \mu_Q, \mu_S) \\ &+ \sum_j n_j(T, \mu_B, \mu_Q, \mu_S) \times \text{Branching Ratio}(j \rightarrow i) \end{aligned} \quad (5)$$

A. Mean-Field HRG (MFHRG)

With the inclusion of short-range repulsive interactions between hadrons via mean-field approach, the effective chemical potential of each particle species gets modified by $\mu_{\text{eff},i} = \mu_i - Kn$, where K is a phenomenological parameter that signifies the strength of the repulsive interaction and n is the number density of the interacting species of particles [31, 32]. The pressure of the mean-field repulsive model is given by:

$$\begin{aligned} P_{\text{MF}}(T, \mu, V) \\ = \pm T \sum_i \frac{g_i}{(2\pi)^3} \int d^3p \ln [1 \pm e^{-(E_i - \mu_{\text{eff},i})/T}] + \mathcal{P}_{M,B,\bar{B}}(n_{M,B,\bar{B}}) \end{aligned} \quad (6)$$

Here, \mathcal{P} is the factor arising from the interacting part, which is necessary to maintain the thermodynamic consistency [31].

$$\begin{aligned} \mathcal{P}_{B\{\bar{B}\}}(n_{B\{\bar{B}\}}) &= \frac{1}{2} K_B n_{B\{\bar{B}\}}^2, \quad (\text{Baryons}) \\ \mathcal{P}_M(n_M) &= \frac{1}{2} K_M n_M^2, \quad (\text{Mesons}) \end{aligned} \quad (7)$$

The above form of interacting pressure is written considering repulsive interactions among meson-meson and baryon(anti-baryon)-baryon(anti-baryon) pairs. Here the total meson number density n_M is calculated as:

$$n_M = \sum_{i \in M} \frac{g_i}{(2\pi)^3} \int \frac{d^3p}{\exp[(E_i - \mu_{\text{eff},i})/T] - 1}. \quad (8)$$

For mesons, $\mu_{\text{eff},i} = \mu_i - K_M n_M$. K_M signifies the strength of the repulsive interactions among the meson-meson pairs. We have a similar equation for baryons and anti-baryon number densities:

$$n_{B\{\bar{B}\}} = \sum_{i \in B\{\bar{B}\}} \frac{g_i}{(2\pi)^3} \int \frac{d^3p}{\exp[(E_i - \mu_{\text{eff},i})/T] + 1}. \quad (9)$$

B and \bar{B} imply baryons and anti-baryons respectively. Here, the effective chemical potential of the i th (anti-)baryon $\mu_{\text{eff},i} = \mu_i - K_B n_{B\{\bar{B}\}}$. The repulsive interactions among the baryon-baryon and antibaryon-antibaryon pairs are given by the same strength parameter K_B . These equations are transcendental in nature and should be solved simultaneously with these two equations Eq.[8-9].

III. METHOD AND DATA ANALYSIS

The mid-rapidity data of hadron yields dN/dY were taken from various experiments at 0-5% centrality (most central) and at different energies. These consist of Pb-Pb collisions in LHC at a collision energy of 2760 GeV [35–38]. We have also included Au-Au collisions at RHIC of 200, 130, 62.4 GeV [39–54], RHIC BES of 39, 27, 19.6, 11.5, 7.7 GeV [55, 56]. and in AGS at 4.85 GeV [57–65].

To extract the chemical freeze-out parameters i.e., T , μ_B , μ_S , μ_Q along with the parameters scaling the strength of the hadron-hadron interaction (K_B and K_M), we have fitted the detected hadron yields with the thermal model estimations. Considering the initial condition of the heavy-ion collision, it is customarily practiced to fix μ_Q and μ_S via two constraint equations. The first constraint is the ratio of net baryon to net charge which remains fixed throughout the collision process considering the isentropic evolution [66].

$$\frac{\sum_i n_i(T, \mu_B, \mu_S, \mu_Q, K_M, K_B) B_i}{\sum_i n_i(T, \mu_B, \mu_S, \mu_Q, K_M, K_B) Q_i} = r \quad (10)$$

One can evaluate this ratio r considering the number of neutrons and protons in the incident nuclei. For heavy nuclei like Au-Au and Pb-Pb, this ratio r is approximately 2.5 [67].

The conservation of strangeness along with the strangeness neutrality imposes another constraint:

$$\sum_i n_i(T, \mu_B, \mu_S, \mu_Q, K_M, K_B) S_i = 0 \quad (11)$$

The rest of the parameters are determined by the χ^2 minimization procedure. The χ^2 is defined as:

$$\chi^2 = \sum_i \frac{\left(\frac{dN_i}{dy} \Big|_{\text{Expt}} - \frac{dN_i}{dy} \Big|_{\text{Model}} \right)^2}{\sigma_i^2} \quad (12)$$

Here, we would like to emphasize that our present analysis focuses exclusively on data from the most central events of the collisions, thus we have chosen not to incorporate the strangeness suppression factor γ_s assuming a state of complete chemical equilibrium. For the present study, we have used data of π^\pm , K^\pm , p , \bar{p} , Λ , $\bar{\Lambda}$, Ξ^\pm , as these are widely available for most of the collision energies. To optimize numerical efficiency and reduce the number of free parameters, we have fixed the K_M at three different values, i.e. 0, 50, and 100 MeV fm⁻³. In the considered HRG spectrum, all confirmed hadronic states up to mass 3 GeV have been included, with masses and branching ratios following the Particle Data Group [68].

The statistics and systematic uncertainties in a given data have been added considering the quadrature method. The variance of the evaluated parameter set for a particular minimization procedure has been calculated from the ± 1 deviation of the minimized χ^2 per degree of freedom [6].

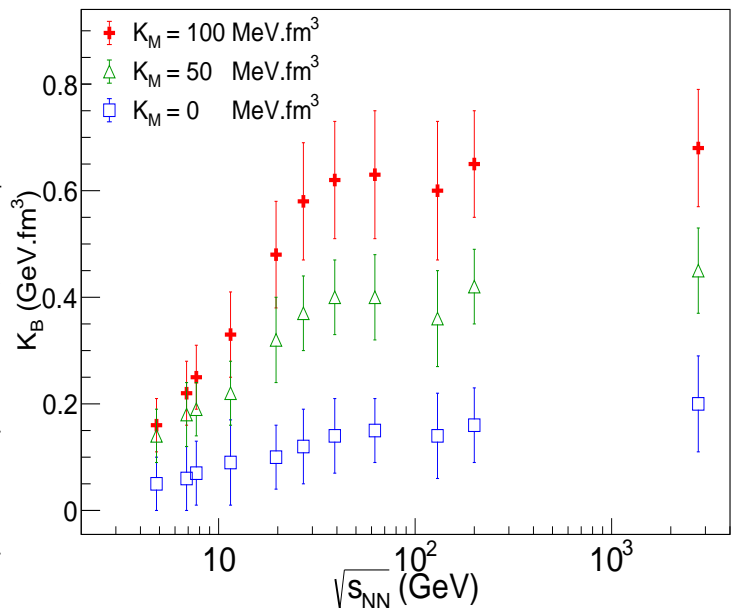


FIG. 1. Results from the fitted set of parameters. Blue, green, and red points are results for K_M values of 0, 50, and 100 MeV fm⁻³ respectively.

IV. RESULT AND DISCUSSION

A. Variation of freeze-out parameters:

We have tabulated the fitted parameter set in Table. I. For convenience, let us first discuss the variation for the mean-field coefficients, as these are the most novel output from our present study. Changes in other freeze-out parameters are commensurate with the variation in these mean-field coefficients. Extraction of both the K_M and K_B becomes numerically challenging due to the slow convergence rate. We have fixed the values of K_M to be 0, 50, and 100 MeV fm⁻³ and examined the corresponding values of K_B . For a fixed value of K_M , the K_B increases with collision energies and remains similar at higher RHIC and LHC energies as shown in Fig. 1. A similar saturation of thermal parameters at higher collision energies has been noticed earlier for temperature and chemical potentials [69, 70]. We have found that even for $K_M = 0.0$ MeV fm⁻³ a non-zero value of K_B helps achieve better χ^2 per degree of freedom while fitting with yield data. With increasing the K_M to 50 and 100 MeV fm⁻³ the values of K_B increases. In the context of heavy-ion collision, the total ensemble of baryons and mesons are connected via the constraints like net strangeness neutrality and a fixed net baryon-to-charge ratio. Along with these constraints, the final yield of mesons is predominantly influenced by the decay of various higher-mass baryon resonances [71]. Consequently, imposing a mean-field repulsion in mesons necessitates a higher value of K_B to restrict the baryon abundances, which eventually affects the final yield of mesons and

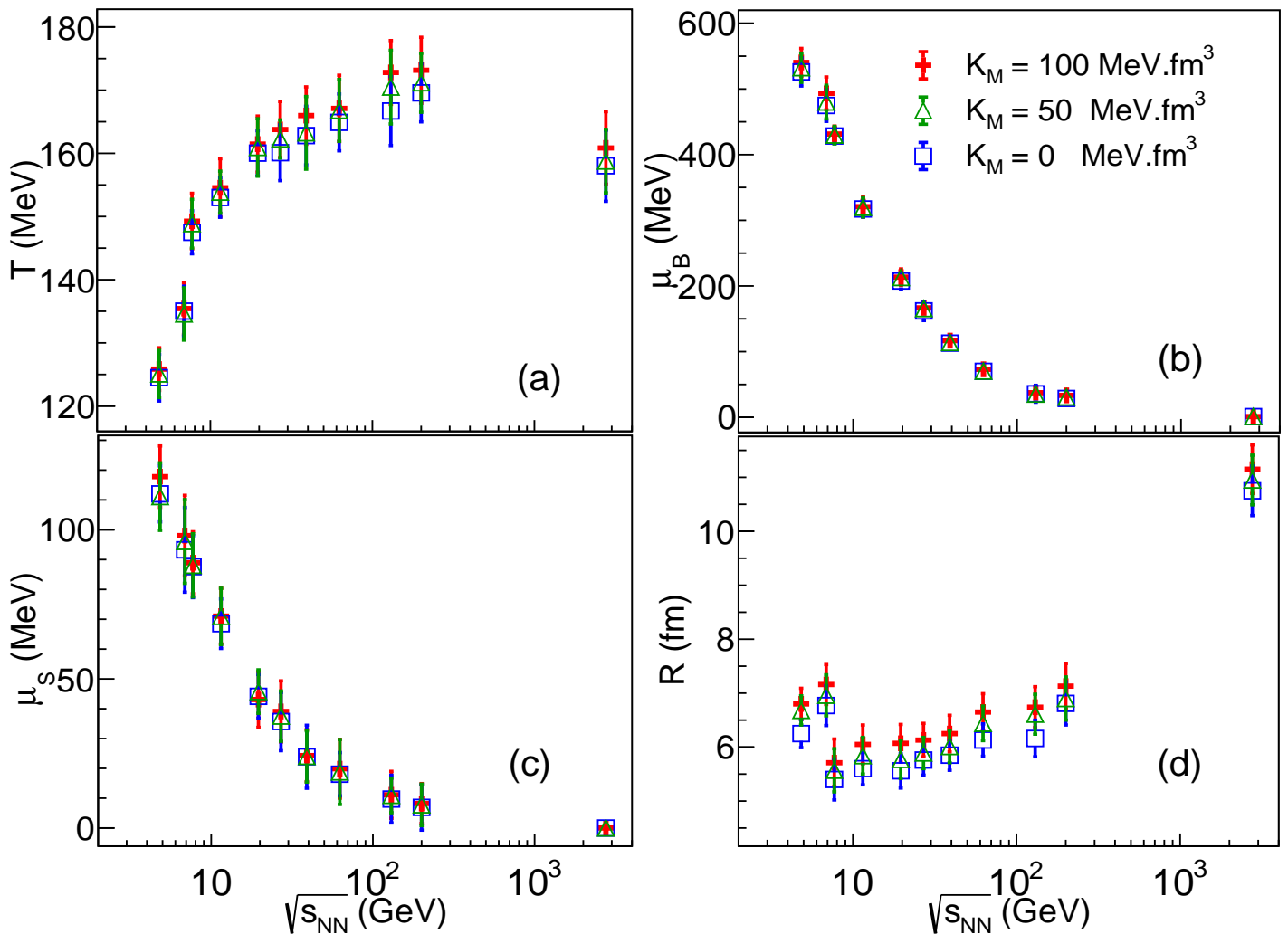


FIG. 2. Fitted set of parameters. Blue, green, and red points are results for K_M values of 0, 50, and 100 MeV fm $^{-3}$ respectively.

validates the required constraints.

Towards the lower collision energy, the medium is mainly baryon-dominated [72], and the effect from the variation of K_M is minimal. However, the system becomes meson dominated with increasing $\sqrt{s_{NN}}$, and the effect of K_M is much more pronounced. We would like to emphasize that for the range of K_M considered, which spans from 0 to 100 MeV fm $^{-3}$, the corresponding K_B values vary between 100 and 800 (considering variances) MeV fm $^{-3}$. These specific values were previously explored in a hydrodynamic simulation that incorporated a hadronic equation of state, as mentioned in Ref. [33]. Furthermore, recent studies conducted using the MFHRG model have also confirmed this range of K_B values as they successfully account for the lattice data of various charge susceptibilities [31, 32, 73].

In the top left panel of Fig. 2, we have shown the variation of freeze-out temperature with collision energy for the three considered values of the mesonic mean-field coefficients K_M as mentioned earlier. For the freeze-out

temperature (T) the difference from considering three different values of K_M seems to be similar to K_B . The differences increase towards high collision energies, following the variation of K_B . For all three values of K_M , the temperature increases with the collision energy and becomes constant around 160 MeV near higher BES energies. We want to iterate here that, although the qualitative behavior is similar to the usual understanding of our freeze-out parametrization within the ideal HRG formalism, the temperature value is slightly higher (~ 5 MeV) than the ideal HRG result. A finite value of the mean-field repulsion parameter restricts the number density which in turn produces a higher T to fit the yields.

The collision energy dependence of the baryon chemical potential is shown in the top right panel. The effect of repulsion is almost negligible on the freeze-out values of μ_B . However, at very lower collision energy, the effect of K_B seems to induce a higher μ_B as the medium is dominated by baryons. The chemical potential is shifted by $K_B n_B$, so a higher value of K_B should be accompa-

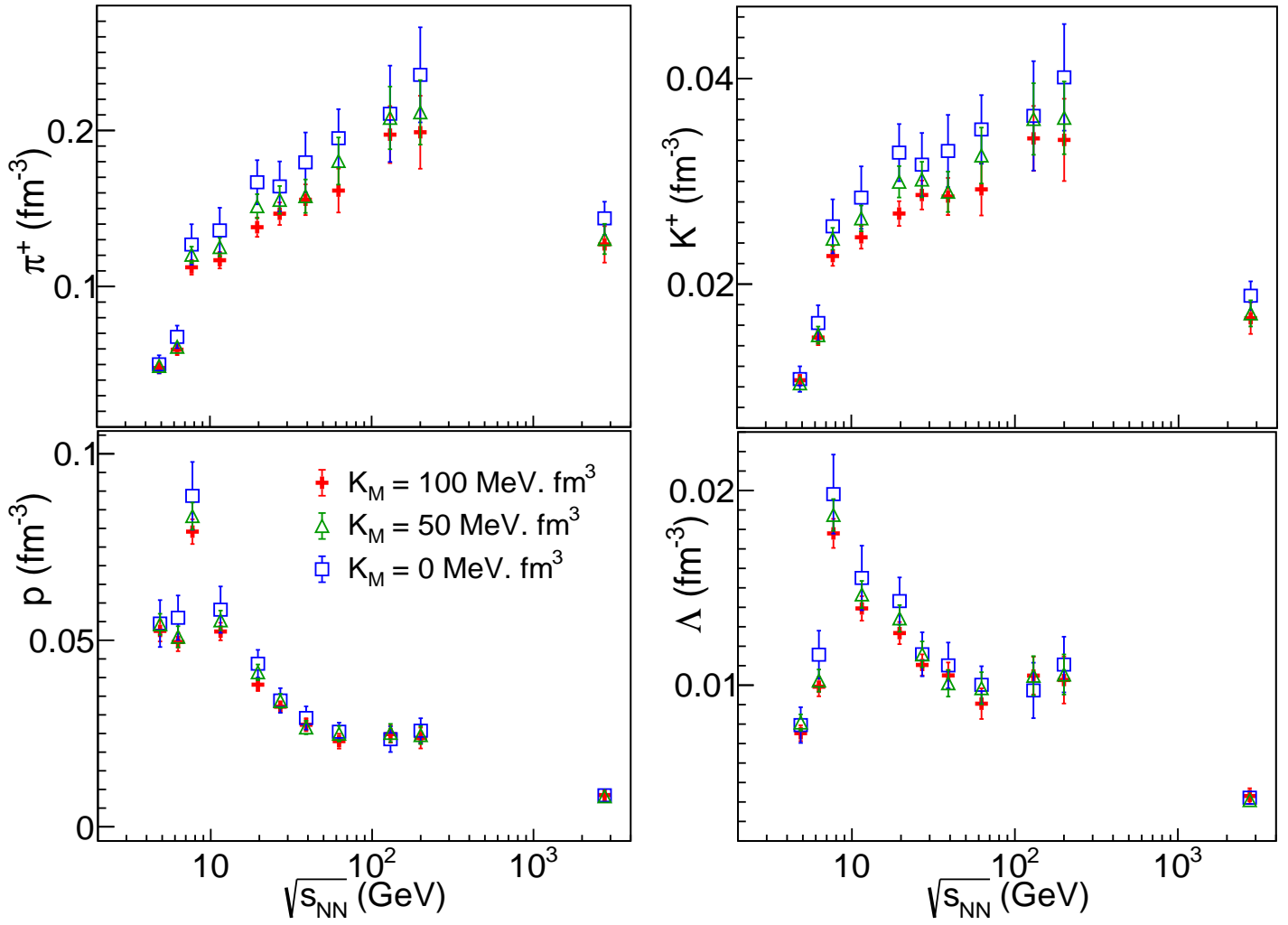


FIG. 3. $\sqrt{s_{NN}}$ variation of the yields of (top left) π^+ , (top right) K^+ , (bottom left) p and (bottom right) Λ . Blue, green, and red points are the results for K_M values of 0, 50, and 100 $\text{MeV} \cdot \text{fm}^{-3}$ respectively. Black points are the experimental data.

nied by a higher μ_B to produce a similar estimation of yields. The general behavior is similar to that of the ideal HRG parametrization. With higher collision energies the baryon stopping diminishes so the medium tends to form with lower net charges (B, Q , and S), which results in a lower value of chemical potentials in the freeze-out parametrization. At lower collision energy this behavior induces a high value of μ_B , which tends to be zero at higher RHIC LHC energy

The strange chemical potential follows the trend of μ_B . A finite μ_B results in the dominance of the hyperons over the anti-hyperons, on the other hand, the strangeness-neutrality constraint demands the cancellation of the net strangeness arising from the baryon sector with that from the meson sector, which demands the μ_S to be proportional to the μ_B . The variance of μ_S is within the uncertainties for the three values of K_M , which indicates that the higher mass strange mesons and baryons have negligible influence from the mean-field repulsion, while

performing the freeze-out parametrization with yields.

The resulting values of the freeze-out volume (which is presented in the freeze-out radius here), are presented in the right bottom panel. A similar non-monotonic behavior with the collision energy was earlier observed from the chemical freeze-out parametrization with ideal HRG in Refs. [6, 74]. The interesting observation here is the higher value of freeze-out radius while we imply a higher value of K_M . A higher value of K_M and K_B suppresses the number density, which in turn results in a higher value of freeze-out radius to fit the yields. One can see that among the above-discussed parameters, the variation of volume with K is much more prominent. It seems that considering the repulsive interaction affects the value of the freeze-out volume mostly as the yield is directly proportional to the volume.

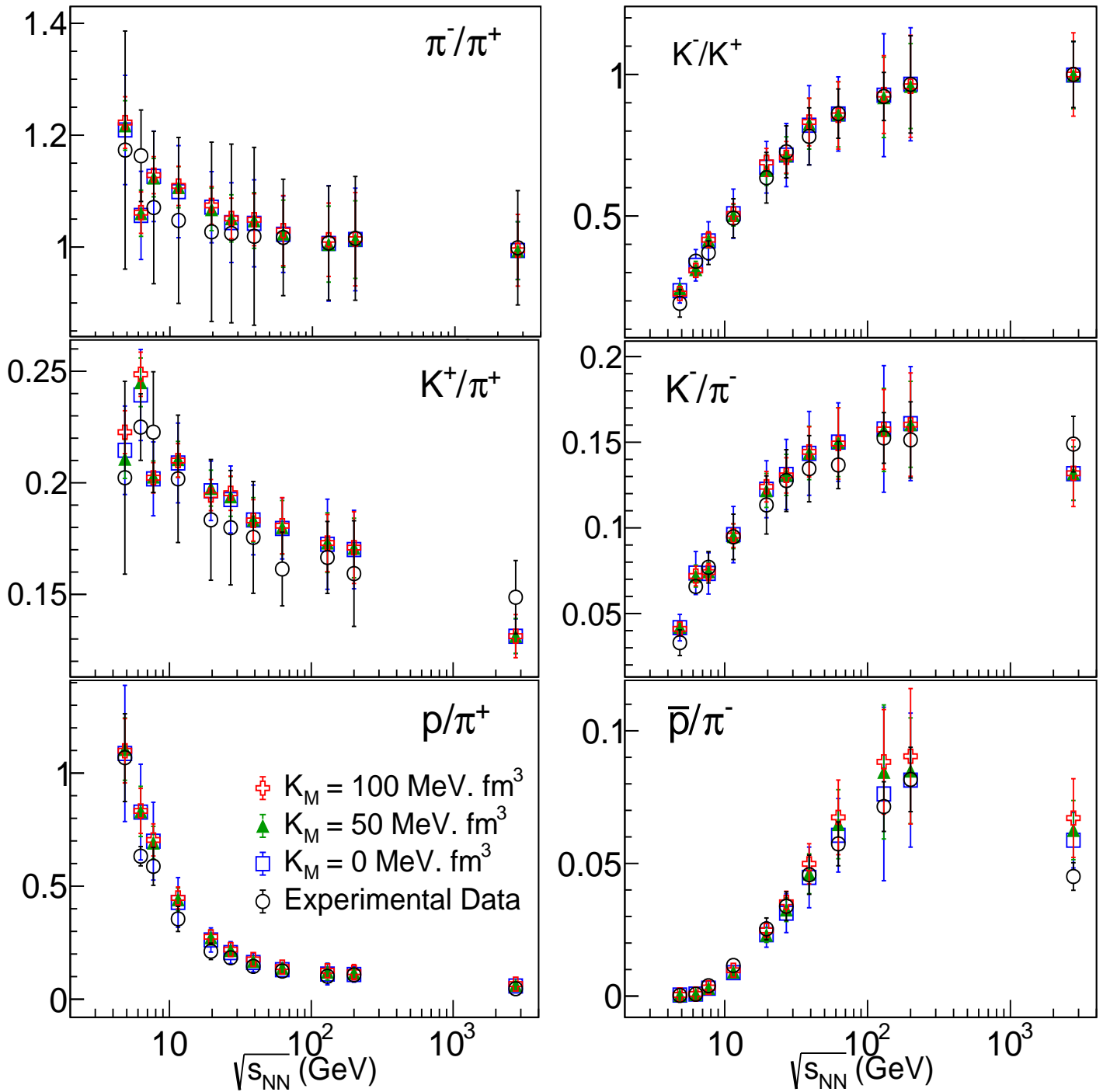


FIG. 4. $\sqrt{s_{NN}}$ variation of the particle to particle ratios π^-/π^+ and K^-/K^+ (top), strange to non-strange meson, K^+/π^+ and K^-/π^- (middle), non-strange baryon to meson, proton to pion (bottom). Blue, green, and red points are the results for K_M values of 0, 50, and 100 MeV fm^{-3} respectively. Black points are the experimental data from Ref. [75].

B. Particle yields from thermal parametrization:

To examine the differences in thermal abundances resulting from different values of K_M , it would be informative to analyze the variations in yields. Fig. 3 displays the number density of pions, kaons, protons, and lambdas,

calculated with the resulting parametrization. The impact of varying K_M is more pronounced for lighter mass pions, while the effect diminishes as the particle mass increases. Baryons with higher masses show negligible variations across the three cases, whereas pions demonstrate more significant alterations when different K_M values are con-

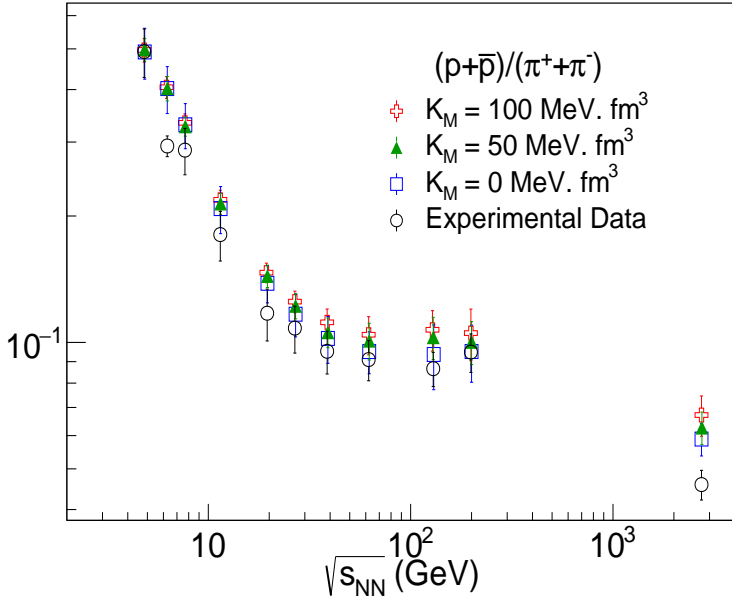


FIG. 5. $\sqrt{s_{NN}}$ variation of the total proton to total pion. Blue, green, and red points are the results for K_M values of 0, 50, and 100 MeV fm^{-3} respectively. Black points are the experimental data from Ref. [75].

sidered.

The effective chemical potential $\mu_{\text{eff},i} = \mu_i - K n_{M,B,\bar{B}}$ is expected to have a significant impact on pions since they carry only electric charge, and the magnitude of μ_Q is much smaller compared to other chemical potentials. Conversely, the effect of this shift diminishes for strange and non-strange baryons, as their respective chemical potentials have larger magnitudes. It is worth noting that the chemical potentials themselves are modified for different K_M values, contributing to the observed variations.

In this context, it is important to consider the decay feed-down effect as well. The total pion density receives a significant contribution from the decay of higher-mass meson and baryon resonances. The suppression of these states is also reflected in the final pion abundance, resulting in substantial variations. This effect is similarly observed for the lowest-mass strange hadron, kaon. On the other hand, baryons receive contributions from higher-mass baryons that are already thermally suppressed, leading to insignificant variations while considering different K_M values.

At this juncture, we want to reiterate that the yield dN/dY is a product of this thermal density and the freeze-out volume dV/dY . A reverse trend was observed for the freeze-out volume in Fig. 2, i.e. a higher value of K_M resulted in higher values of freeze-out volume. The cumulative effect of these two ensures the agreement between the yield data and our thermal model estimation. This indicates that the resulting parameters (especially freeze-out volume and K_B) are dependent on each other and on the values of K_M . In our present study, it becomes

challenging to decouple this systemic dependency.

C. Particle ratios:

It would be interesting to estimate various particle ratios and compare them with those from the experimental data. Along with checking the efficacy of our parameterization, this will also examine the effect of various choices of K_M on thermal yields. Here we shall discuss some of the important particle ratios from various sectors.

The ratios of π^-/π^+ and K^-/K^+ as a function of $\sqrt{s_{NN}}$ are depicted in the upper panel of Fig. 4. Our parameterization successfully reproduces the observed variation of the experimental data. The pion ratio is greater than unity at lower $\sqrt{s_{NN}}$ due to the higher abundance of neutrons in the colliding nuclei, which induces an isospin asymmetry favoring π^- . However, this asymmetry diminishes at higher RHIC and LHC energies, resulting in similar yields of π^- and π^+ . In the case of kaons, the variation follows the trend of μ_S . At lower collision energies, the positively charged kaon (K^+) becomes more abundant than the negatively charged kaon (K^-) to maintain strangeness neutrality. As the collision energy increases, this effect disappears, and the yields of particles and antiparticles become equal at the LHC. The qualitative behavior is the same for all three values of K_M . It seems that the effect of K_M does not result in the large variation of the mentioned ratio.

In the context of the heavy-ion collision, the strange to non-strange ratios signify the relative abundance of strangeness and portray the degree of equilibration for the strange sector [76]. Deviations from the equilibrium values have earlier been observed for non-central collisions, which necessitates the use of a strangeness saturation factor γ_S [70]. Being the lightest strange to non-strange particle, the ratio K^+/π^+ and K^-/π^- are widely studied within the thermal model. The explanation of the non-monotonic behavior of the K^+/π^+ was discussed as a signature of the thermalization in the strange sector and a possible existence of initial partonic state [77–81]. Although these details are beyond the scope of the present thermal model, our parameterization suitably explains the data for all three values of K_M in the middle panel of Fig. 4. Although, there is not much variation among the estimations from the three cases, indicating that these ratios have a weak dependence on the variation of K_M and K_B .

We have shown the proton-to-pion ratio in the bottom panel of Fig. 4. As we have separately used two different mean-field coefficients K_M and K_B for the meson and baryon sectors separately, this ratio will portray their effect on the respective variation. We have plotted p/π^+ and \bar{p}/π^- to nullify the effect of the charge chemical potential. In the context of heavy-ion collision, the abundance of pions is mainly dominated by the temperature as they are the lowest mass hadrons, whereas the protons mimic the variation of exponential of μ_B/T . At lower

collision energy the medium is dominated by the baryons due to the baryon stopping, whereas at higher collision energies the system is dominated by the mesons, and changes from a baryon-dominated freeze-out to meson-dominated freeze-out occurs [72]. This phenomenon explains the variation observed in the proton to π^+ ratio. On the other hand, the production of anti-proton increases as the collision energy increases and at high RHIC and LHC energies, the two ratio becomes similar. Here the values of the p/π^+ ratio increase as we increase the K_M for a given collision energy. A higher value of K_M suppresses the abundance of pions and produces a higher value of the ratio.

To quantify the impact of the various choice of repulsive parameters K_M and K_B in the particle ratios, we have plotted the total proton ($p + \bar{p}$) abundance normalized to total pion ($\pi^+ + \pi^-$) in Fig. 5. This ratio has a larger impact from various choices of K_M than that of the individual ratios, as it signifies the relative abundance of the lowest mass baryons to that of the lowest mass mesons. The parametrization for $K_M = 0$ seems to agree with the data better than the other choices. At the freeze-out parametrization, one should not expect much variation in the baryon yield from the variation of K_B due to their heavier masses, on the contrary, the pion yields get significantly suppressed for a higher value of K_M due to the lower masses. This results in the variation shown as the ratio $((p + \bar{p})/(\pi^+ + \pi^-))$, as for a given collision energy it increases for a higher value of K_M . The difference is much more pronounced at higher collision energies, as the thermal medium is meson dominated, so the different choices of K_M produce a larger effect.

Motivated by the fact that the ratio corresponding to the total proton yield to pions gets significant variation from the values of mean-field parameter K_M , we have investigated their impact on the ratios of susceptibilities calculated with the freeze-out parameterization. The n th order susceptibility is defined as:

$$\chi_x^n = \frac{1}{VT^3} \frac{\partial^n (\ln Z)}{\partial (\frac{\mu_x}{T})^n} \quad (13)$$

where μ_x is the chemical potential for conserved charge x . The susceptibilities would be related to the cumulants measured in the heavy-ion collisions as:

$$VT^3 \chi_x^n = C_n. \quad (14)$$

As we have fixed the K_M and fitted the mean-field coefficient K_B , it will be interesting to check the variance in the baryon cumulant ratios. We have calculated these cumulants within the Boltzmann approximation as it provides a reasonable baseline for the massive hadrons and resonances (except π) along the chemical freeze-out boundary [71], as $m_i - \mu_i \gg T$ at the respective freeze-out parametrization. Within this consideration, we can approximate the interacting partition functions in the Boltzmann limit and calculate the χ_B^n [31, 82]. The differences arising from various values of the K_M increase

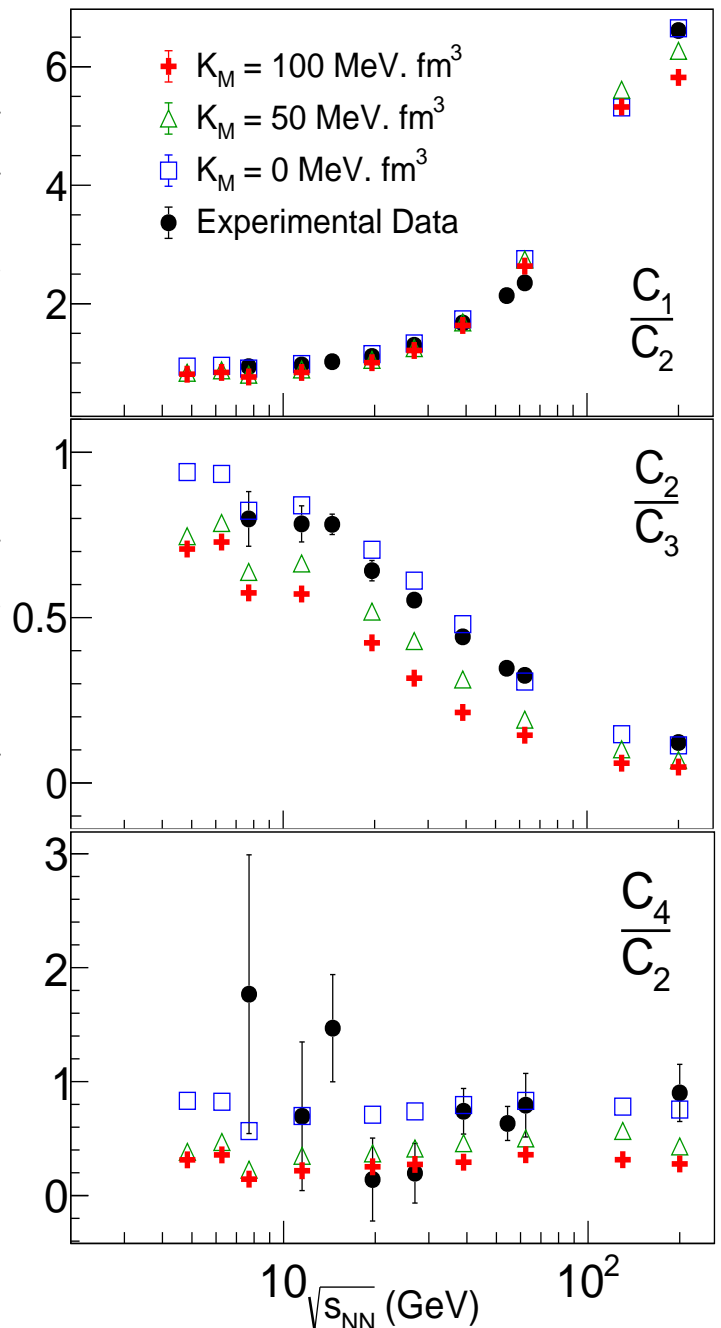


FIG. 6. $\sqrt{s_{NN}}$ variation of the cumulant ratios C_2/C_1 (top), C_3/C_2 (middle) and C_4/C_2 (bottom). Blue, green, and red points are the results for K_M values of 0, 50, and 100 MeV fm^{-3} respectively. Black points are the experimental data from Ref. [75].

as we move to ratios of higher-order cumulants. The effect is negligible for C_2/C_1 , while C_3/C_2 and C_4/C_2 decrease as we fix the K_M to higher values. As we imply a higher value of K_M , it produces a higher value of K_B as discussed earlier in Sec. IV A, which translates into these differences. We want to mention that the ratio C_4/C_2 is 1 at all collision energy for the ideal HRG case, whereas the

impact of interaction gives rise to the observed variation.

As a baseline, we have also plotted results for the net proton cumulants estimations from STAR collaboration [75, 83]. For simplification, we have not mimicked the experimental specification like p_T cut, decay feed-down into the cumulants calculations. Although the effect of decay feed-down and p_T cut-off have been found to be minimal earlier [82, 84, 85]. We want to reiterate that we have calculated the baryon cumulants ratios, which is different from the net-proton ratios. Although the qualitative behavior is similar, the quantitative difference between these two increases for higher order cumulant ratios [75]. The non-monotonic variation of C_4/C_2 is not well captured in the thermal model estimation, although the results vary from the ideal baseline of 1. The C_2/C_1 and C_3/C_2 estimations agree with the data for $K_M = 50 \text{ MeV fm}^{-3}$, there are larger deviation for C_4/C_2 , which seem to match for higher values of K_M . This behavior suggests that a complete study of the net-proton cumulants with experimental constraints might restrict the variation of K_M and K_B both.

V. SUMMARY

Recent advancements in incorporating repulsive interactions between baryons and mesons in the hadron resonance gas (HRG) model have established it as a suitable candidate for providing a bulk description of the QCD medium below the transition temperature. Phenomenological descriptions such as the excluded volume HRG and van der Waals HRG models consider parameters such as a hard-core impenetrable radius of the hadrons. On the other hand, the mean-field repulsive HRG model (MFHRG) provides a robust representation of the medium by accounting for a density-dependent interaction strength. However, this model requires the inclusion of parameters such as K_B and K_M to scale the interaction strength among baryons and mesons, which can be appropriately estimated using bulk observables obtained from lattice QCD [31, 32]. It is crucial to apply this mean-field repulsive model to analyze data from heavy-ion collision experiments and assess its effectiveness in comparison to other counterparts such as the ideal HRG, evHRG, vdWHRG, and so on. Exploring the chemical freeze-out surface provides a foundation for investigating the collision energy dependence of the repulsive interaction strength by estimating K_M and K_B .

To parametrize the chemical freeze-out surface, we utilized the p_T -integrated mid-rapidity yield dN/dY data for pions, kaons, protons, Λ , and Ξ in the most central collisions. The collision energy range available in AGS (4.85 GeV), RHIC-BES, and LHC (2.76 TeV) was analyzed. Given that the parameters K_B and K_M are interdependent due to relevant constraints and decay feed-down

effects, evaluating them independently can lead to larger numerical variances. To address this issue, we fixed K_M at three representative values (0, 50, and 100 MeV.fm^{-3}) and performed a χ^2 fitting to determine the remaining parameters: T , μ_B , μ_Q , μ_S , K_B , and the freeze-out radius R .

While the values of K_B were found to be finite and influenced the goodness of fit, the other parameters were consistent with those obtained from the ideal HRG model. Notably, K_B increases with collision energy and becomes significantly higher at higher $\sqrt{s_{NN}}$. It is intriguing to observe that the values of K_B obtained from this freeze-out analysis are similar to those from earlier studies using the mean-field approach. The agreement between the estimation of K_B from lattice QCD-motivated studies [31, 32, 73, 86] and our analysis underscores the effectiveness of this model in describing the bulk properties of the created medium in heavy-ion collisions.

Studying the influence of repulsive interactions on the thermal abundance of different states was crucial. While the effect of finite K_M and K_B values on the number density of massive strange hadrons and baryons was not significant, it played a more prominent role in the case of pions. Particle ratios within the same sector, such as meson-to-meson and baryon-to-baryon ratios were less affected by variations in K_M and K_B . However, the proton-to-pion ratios exhibited significant variations. Consequently, the total proton to total pion ratio became a subject of investigation, as it appeared to be strongly dependent on the values of K_M . Additionally, we explored the ratio of baryon susceptibilities using this freeze-out parameterization, as these susceptibilities are linked to net-proton cumulants measured in heavy-ion collisions. While our freeze-out parametrization was based on yields, there was a general agreement between our estimations of baryon cumulant ratios and the measurements of net-proton for lower orders. However, discrepancies arose when considering fourth-order cumulants. Proper treatment of cumulant ratios requires accounting for decay feed-down effects and implementing p_T cuts within the framework of this mean-field repulsive HRG model. This consideration will be essential for future studies, particularly in the context of energy available in BES-II, HADES, and CBM experiments.

ACKNOWLEDGEMENTS

D.B expresses gratitude to Sayantan Sharma, Aman Kanojia, Somenath Pal and Hiranmaya Mishra for engaging and fruitful discussions. D.B. would like to express sincere gratitude for the support received from NISER, Bhubaneswar, with special thanks to A. Jaiswal for the kind assistance and hospitality during the visit, where the majority of this work was performed.

TABLE I.

Particle+Anti Particle: π, K, P, Λ, Ξ , centrality: 0-5%, Constrain: $netB/netQ = 2.5$ and $netS = 0.0$							
$\sqrt{s_{NN}}$ (GeV)	κ_M (MeV.fm ⁻³)	κ_B (GeV.fm ⁻³)	T_{ch} (MeV)	μ_B (MeV)	μ_S (MeV)	R(fm)	χ^2/ndf
4.83	0	0.03(0.05)	124.50(3.70)	526.02(21.50)	112.02(9.39)	6.25(0.26)	1.11
	50	0.16(0.05)	125.08(3.73)	532.34(21.39)	111.11(10.28)	6.68(0.27)	1.72
	100	0.18(0.0)	125.85(3.38)	540.40(22.24)	117.59(11.32)	6.80(0.29)	1.67
6.27	0	0.04(0.04)	131.03(2.95)	454.88(14.25)	93.27(14.20)	6.77(0.37)	2.60
	50	0.18(0.06)	130.57(3.13)	450.07(14.91)	96.07(13.50)	6.96(0.38)	2.81
	100	0.22(0.05)	131.43(2.95)	463.34(17.58)	98.04(14.04)	7.16(0.37)	2.65
7.7	0	0.07(0.06)	147.50(3.40)	428.35(11.53)	87.62(10.38)	5.40(0.38)	2.06
	50	0.19(0.08)	148.87(3.85)	429.77(12.07)	88.05(10.40)	5.57(0.40)	2.06
	100	0.25(0.09)	149.26(4.41)	431.36(13.29)	88.93(10.60)	5.71(0.44)	2.06
11.5	0	0.07(0.08)	153.01(3.13)	317.27(12.37)	68.51(8.30)	5.60(0.30)	1.56
	50	0.22(0.10)	153.85(3.33)	319.68(15.63)	70.94(9.33)	5.84(0.34)	1.57
	100	0.33(0.10)	154.55(4.60)	320.75(14.59)	71.05(9.45)	6.05(0.36)	1.54
19.6	0	0.10(0.06)	160.03(3.56)	207.65(12.45)	44.15(7.33)	5.56(0.32)	1.18
	50	0.32(0.12)	160.93(4.55)	212.82(12.51)	45.75(9.34)	5.77(0.35)	1.19
	100	0.48(0.18)	161.46(4.44)	213.43(09.45)	43.08(7.29)	6.07(0.35)	1.20
27.0	0	0.12(0.07)	160.10(3.42)	162.02(14.70)	35.70(9.77)	5.76(0.28)	1.07
	50	0.37(0.12)	162.27(3.02)	165.41(10.69)	37.52(10.26)	5.89(0.29)	0.99
	100	0.58(0.16)	163.77(4.43)	166.64(10.39)	39.08(8.43)	6.13(0.31)	1.09
39.0	0	0.12(0.07)	160.81(4.64)	112.91(10.75)	23.89(10.56)	5.85(0.28)	0.54
	50	0.42(0.12)	163.24(5.75)	113.83(08.94)	24.00(8.74)	6.01(0.30)	0.47
	100	0.65(0.18)	165.98(4.53)	116.71(08.57)	24.28(8.62)	6.25(0.34)	0.43
62.4	0	0.10(0.05)	164.89(4.50)	69.91(8.68)	18.04(7.25)	6.13(0.30)	1.34
	50	0.38(0.09)	166.80(4.90)	70.21(7.53)	18.79(9.87)	6.44(0.32)	1.23
	100	0.59(0.15)	167.11(5.23)	73.07(7.29)	19.87(10.90)	6.65(0.34)	1.17
130.0	0	0.14(0.08)	166.70(5.46)	35.79(12.85)	9.70(8.00)	6.16(0.34)	1.62
	50	0.28(0.10)	170.48(5.83)	35.27(8.48)	10.93(7.88)	6.61(0.37)	1.06
	100	0.55(0.10)	172.80(5.33)	37.39(6.08)	11.12(5.80)	6.71(0.38)	1.16
200.0	0	0.14(0.07)	169.57(4.59)	28.59(7.61)	6.91(7.61)	6.81(0.40)	1.03
	50	0.42(0.13)	171.17(4.67)	30.72(7.73)	7.76(6.70)	6.90(0.40)	0.69
	100	0.61(0.24)	173.15(5.22)	33.34(8.74)	8.20(6.97)	7.13(0.42)	0.57
2760.00	0	0.20(0.11)	158.03(5.62)	1.97(1.30)	0.0	10.75(0.46)	2.54
	50	0.45(0.18)	158.77(5.03)	1.11(0.54)	0.0	10.95(0.46)	2.31
	100	0.66(0.20)	159.85(5.74)	1.06(0.74)	0.0	11.15(0.45)	2.43

- [1] R. Stock, *Relativistic Nucleus-Nucleus Collisions and the QCD Matter Phase Diagram*, Springer International Publishing, Cham, 2020, pp. 311–453. doi:10.1007/978-3-030-38207-0_7. URL https://doi.org/10.1007/978-3-030-38207-0_7
- [2] J. Cleymans, H. Satz, Thermal hadron production in high-energy heavy ion collisions, *Z. Phys. C* 57 (1993) 135–148. arXiv:hep-ph/9207204, doi:10.1007/BF01555746.
- [3] J. Cleymans, K. Redlich, Unified description of freezeout parameters in relativistic heavy ion collisions, *Phys. Rev. Lett.* 81 (1998) 5284–5286. arXiv:nucl-th/9808030, doi:10.1103/PhysRevLett.81.5284.
- [4] J. Cleymans, K. Redlich, Chemical and thermal freezeout parameters from 1-A/GeV to 200-A/GeV, *Phys. Rev. C* 60 (1999) 054908. arXiv:nucl-th/9903063, doi:10.1103/PhysRevC.60.054908.
- [5] F. Becattini, J. Cleymans, A. Keranen, E. Suhonen, K. Redlich, Features of particle multiplicities and strangeness production in central heavy ion collisions between 1.7A-GeV/c and 158A-GeV/c, *Phys. Rev. C* 64 (2001) 024901. arXiv:hep-ph/0002267, doi:10.1103/PhysRevC.64.024901.
- [6] A. Andronic, P. Braun-Munzinger, J. Stachel, Hadron production in central nucleus-nucleus collisions at chemical

- freeze-out, Nucl. Phys. A772 (2006) 167–199. [arXiv:nucl-th/0511071](#), [doi:10.1016/j.nuclphysa.2006.03.012](#).
- [7] A. Andronic, P. Braun-Munzinger, J. Stachel, Thermal hadron production in relativistic nuclear collisions: The Hadron mass spectrum, the horn, and the QCD phase transition, Phys. Lett. B673 (2009) 142–145, [Erratum: Phys. Lett. B678,516(2009)]. [arXiv:0812.1186](#), [doi:10.1016/j.physletb.2009.02.014](#), [10.1016/j.physletb.2009.06.021](#).
- [8] R. Dashen, S.-K. Ma, H. J. Bernstein, S Matrix formulation of statistical mechanics, Phys. Rev. 187 (1969) 345–370. [doi:10.1103/PhysRev.187.345](#).
- [9] M. Prakash, M. Prakash, R. Venugopalan, G. Welke, Nonequilibrium properties of hadronic mixtures, Phys. Rept. 227 (1993) 321–366. [doi:10.1016/0370-1573\(93\)90092-R](#).
- [10] R. Bellwied, S. Borsanyi, Z. Fodor, S. D. Katz, A. Pasztor, C. Ratti, K. K. Szabo, Fluctuations and correlations in high temperature QCD, Phys. Rev. D 92 (11) (2015) 114505. [arXiv:1507.04627](#), [doi:10.1103/PhysRevD.92.114505](#).
- [11] A. Bazavov, et al., Strangeness at high temperatures: from hadrons to quarks, Phys. Rev. Lett. 111 (2013) 082301. [arXiv:1304.7220](#), [doi:10.1103/PhysRevLett.111.082301](#).
- [12] G. D. Yen, M. I. Gorenstein, W. Greiner, S.-N. Yang, Excluded volume hadron gas model for particle number ratios in A+A collisions, Phys. Rev. C56 (1997) 2210–2218. [arXiv:nucl-th/9711062](#), [doi:10.1103/PhysRevC.56.2210](#).
- [13] A. Andronic, P. Braun-Munzinger, J. Stachel, M. Winn, Interacting hadron resonance gas meets lattice QCD, Phys. Lett. B718 (2012) 80–85. [arXiv:1201.0693](#), [doi:10.1016/j.physletb.2012.10.001](#).
- [14] D. H. Rischke, M. I. Gorenstein, H. Stoecker, W. Greiner, Excluded volume effect for the nuclear matter equation of state, Z. Phys. C51 (1991) 485–490. [doi:10.1007/BF01548574](#).
- [15] R. Hagedorn, J. Rafelski, Hot Hadronic Matter and Nuclear Collisions, Phys. Lett. 97B (1980) 136. [doi:10.1016/0370-2693\(80\)90566-3](#).
- [16] V. V. Begun, M. Gazdzicki, M. I. Gorenstein, Hadron-resonance gas at freeze-out: Reminder on the importance of repulsive interactions, Phys. Rev. C88 (2) (2013) 024902. [arXiv:1208.4107](#), [doi:10.1103/PhysRevC.88.024902](#).
- [17] S. K. Tiwari, P. K. Srivastava, C. P. Singh, Description of Hot and Dense Hadron Gas Properties in a New Excluded-Volume model, Phys. Rev. C85 (2012) 014908. [arXiv:1111.2406](#), [doi:10.1103/PhysRevC.85.014908](#).
- [18] M. I. Gorenstein, A. P. Kostyuk, Y. D. Krivenko, Van der Waals excluded volume model of multicomponent hadron gas, J. Phys. G 25 (1999) L75–L83. [arXiv:nucl-th/9906068](#), [doi:10.1088/0954-3899/25/9/102](#).
- [19] V. Vovchenko, H. Stoecker, Examination of the sensitivity of the thermal fits to heavy-ion hadron yield data to the modeling of the eigenvolume interactions, Phys. Rev. C 95 (4) (2017) 044904. [arXiv:1606.06218](#), [doi:10.1103/PhysRevC.95.044904](#).
- [20] J. Noronha-Hostler, H. Ahmad, J. Noronha, C. Greiner, Particle Ratios as a Probe of the QCD Critical Temperature, Phys. Rev. C 82 (2010) 024913. [arXiv:0906.3960](#), [doi:10.1103/PhysRevC.82.024913](#).
- [21] V. Vovchenko, H. Stöcker, Surprisingly large uncertainties in temperature extraction from thermal fits to hadron yield data at LHC, J. Phys. G 44 (5) (2017) 055103. [arXiv:1512.08046](#), [doi:10.1088/1361-6471/aa6409](#).
- [22] P. Alba, V. Vovchenko, M. I. Gorenstein, H. Stoecker, Flavor-dependent eigenvolume interactions in a hadron resonance gas, Nucl. Phys. A 974 (2018) 22–34. [arXiv:1606.06542](#), [doi:10.1016/j.nuclphysa.2018.03.007](#).
- [23] V. Vovchenko, D. V. Anchishkin, M. I. Gorenstein, Particle number fluctuations for the van der Waals equation of state, J. Phys. A 48 (30) (2015) 305001. [arXiv:1501.03785](#), [doi:10.1088/1751-8113/48/30/305001](#).
- [24] V. Vovchenko, D. V. Anchishkin, M. I. Gorenstein, Van der Waals Equation of State with Fermi Statistics for Nuclear Matter, Phys. Rev. C 91 (6) (2015) 064314. [arXiv:1504.01363](#), [doi:10.1103/PhysRevC.91.064314](#).
- [25] S. Samanta, B. Mohanty, Criticality in a Hadron Resonance Gas model with the van der Waals interaction, Phys. Rev. C 97 (1) (2018) 015201. [arXiv:1709.04446](#), [doi:10.1103/PhysRevC.97.015201](#).
- [26] N. Sarkar, P. Ghosh, van der Waals hadron resonance gas and QCD phase diagram, Phys. Rev. C 98 (1) (2018) 014907. [arXiv:1807.02948](#), [doi:10.1103/PhysRevC.98.014907](#).
- [27] N. Sarkar, Investigating the impact of extra resonance states in the van der Waals Hadron Resonance Gas Model (4 2023). [arXiv:2304.11914](#).
- [28] K. A. Olive, The Thermodynamics of the Quark - Hadron Phase Transition in the Early Universe, Nucl. Phys. B 190 (1981) 483–503. [doi:10.1016/0550-3213\(81\)90444-2](#).
- [29] K. A. Olive, THE QUARK - HADRON TRANSITION IN SYSTEMS WITH NET BARYON NUMBER, Nucl. Phys. B 198 (1982) 461–473. [doi:10.1016/0550-3213\(82\)90335-2](#).
- [30] J. I. Kapusta, K. A. Olive, Thermodynamics of Hadrons: Delimiting the Temperature, Nucl. Phys. A 408 (1983) 478–494. [doi:10.1016/0375-9474\(83\)90241-5](#).
- [31] P. Huovinen, P. Petreczky, Hadron resonance gas with repulsive interactions and fluctuations of conserved charges, Phys. Lett. B 777 (2018) 125–130. [arXiv:1708.00879](#), [doi:10.1016/j.physletb.2017.12.001](#).
- [32] G. Kadam, H. Mishra, Hadron resonance gas with repulsive mean field interaction: Thermodynamics and transport properties, Phys. Rev. D 100 (7) (2019) 074015. [arXiv:1907.02199](#), [doi:10.1103/PhysRevD.100.074015](#).
- [33] J. Sollfrank, P. Huovinen, M. Kataja, P. V. Ruuskanen, M. Prakash, R. Venugopalan, Hydrodynamical description of 200-A/GeV/c S + Au collisions: Hadron and electromagnetic spectra, Phys. Rev. C 55 (1997) 392–410. [arXiv:nucl-th/9607029](#), [doi:10.1103/PhysRevC.55.392](#).
- [34] R. Hagedorn, Statistical thermodynamics of strong interactions at high-energies, Nuovo Cim. Suppl. 3 (1965) 147–186.
- [35] B. Abelev, et al., Pion, Kaon, and Proton Production in Central Pb–Pb Collisions at $\sqrt{s_{NN}} = 2.76$ TeV, Phys. Rev. Lett. 109 (2012) 252301. [arXiv:1208.1974](#), [doi:10.1103/PhysRevLett.109.252301](#).
- [36] B. B. Abelev, et al., K_S^0 and Λ production in Pb-Pb collisions at $\sqrt{s_{NN}} = 2.76$ TeV, Phys. Rev. Lett. 111 (2013) 222301. [arXiv:1307.5530](#), [doi:10.1103/PhysRevLett.111.222301](#).
- [37] B. B. Abelev, et al., Multi-strange baryon production at mid-rapidity in Pb-Pb collisions at $\sqrt{s_{NN}} = 2.76$ TeV, Phys. Lett. B728 (2014) 216–227, [Erratum: Phys. Lett. B734,409(2014)]. [arXiv:](#)

- 1307.5543, doi:10.1016/j.physletb.2014.05.052, 10.1016/j.physletb.2013.11.048.
- [38] B. Abelev, et al., Centrality dependence of π , K, p production in Pb-Pb collisions at $\sqrt{s_{NN}} = 2.76$ TeV, Phys. Rev. C88 (2013) 044910. arXiv:1303.0737, doi:10.1103/PhysRevC.88.044910.
- [39] L. Kumar, STAR Results from the RHIC Beam Energy Scan-I, Nucl. Phys. A904-905 (2013) 256c–263c. arXiv:1211.1350, doi:10.1016/j.nuclphysa.2013.01.070.
- [40] S. Das, Centrality dependence of freeze-out parameters from the beam energy scan at STAR, Nucl. Phys. A904-905 (2013) 891c–894c. arXiv:1210.6099, doi:10.1016/j.nuclphysa.2013.02.158.
- [41] C. Adler, et al., Midrapidity Lambda and anti-Lambda production in Au + Au collisions at $s(NN)^{1/2} = 130$ -GeV, Phys. Rev. Lett. 89 (2002) 092301. arXiv:nucl-ex/0203016, doi:10.1103/PhysRevLett.89.092301.
- [42] J. Adams, et al., Multistrange baryon production in Au-Au collisions at $S(NN)^{1/2} = 130$ GeV, Phys. Rev. Lett. 92 (2004) 182301. arXiv:nucl-ex/0307024, doi:10.1103/PhysRevLett.92.182301.
- [43] X. Zhu, Measurements of K_s^0 , Λ and Ξ from Au+Au collisions at $\sqrt{s_{NN}} = 7.7, 11.5$ and 39 GeV in STAR, Acta Phys. Polon. Supp. 5 (2012) 213–218. arXiv:1203.5183, doi:10.5506/APhysPolBSupp.5.213.
- [44] F. Zhao, Beam Energy Dependence of Strange Hadron Production from STAR at RHIC, J. Phys. Conf. Ser. 509 (2014) 012085. doi:10.1088/1742-6596/509/1/012085.
- [45] L. Kumar, Systematics of Kinetic Freeze-out Properties in High Energy Collisions from STAR, Nucl. Phys. A931 (2014) 1114–1119. arXiv:1408.4209, doi:10.1016/j.nuclphysa.2014.08.085.
- [46] S. Das, Study of freeze-out dynamics in STAR at RHIC Beam Energy Scan Program, J. Phys. Conf. Ser. 509 (2014) 012066. arXiv:1402.0255, doi:10.1088/1742-6596/509/1/012066.
- [47] B. I. Abelev, et al., Systematic Measurements of Identified Particle Spectra in pp, d^+ Au and Au+Au Collisions from STAR, Phys. Rev. C79 (2009) 034909. arXiv:0808.2041, doi:10.1103/PhysRevC.79.034909.
- [48] M. M. Aggarwal, et al., Strange and Multi-strange Particle Production in Au+Au Collisions at $\sqrt{s_{NN}} = 62.4$ GeV, Phys. Rev. C83 (2011) 024901. arXiv:1010.0142, doi:10.1103/PhysRevC.83.024901.
- [49] B. I. Abelev, et al., Measurements of phi meson production in relativistic heavy-ion collisions at RHIC, Phys. Rev. C79 (2009) 064903. arXiv:0809.4737, doi:10.1103/PhysRevC.79.064903.
- [50] K. Adcox, et al., Measurement of the Lambda and anti-Lambda particles in Au+Au collisions at $s(NN)^{1/2} = 130$ -GeV, Phys. Rev. Lett. 89 (2002) 092302. arXiv:nucl-ex/0204007, doi:10.1103/PhysRevLett.89.092302.
- [51] C. Adler, et al., Midrapidity phi production in Au + Au collisions at $s_{NN} = 130$ -GeV, Phys. Rev. C65 (2002) 041901. doi:10.1103/PhysRevC.65.041901.
- [52] J. Adams, et al., Scaling Properties of Hyperon Production in Au+Au Collisions at $s^{1/2} = 200$ -GeV, Phys. Rev. Lett. 98 (2007) 062301. arXiv:nucl-ex/0606014, doi:10.1103/PhysRevLett.98.062301.
- [53] J. Adams, et al., phi meson production in Au + Au and p+p collisions at $s(NN)^{1/2} = 200$ -GeV, Phys. Lett. B612 (2005) 181–189. arXiv:nucl-ex/0406003, doi:10.1016/j.physletb.2004.12.082.
- [54] L. Kumar, Centrality dependence of freeze-out parameters from Au+Au collisions at $\sqrt{s_{NN}} = 7.7, 11.5$ and 39 GeV, Central Eur. J. Phys. 10 (2012) 1274–1277. arXiv:1201.4203, doi:10.2478/s11534-012-0097-9.
- [55] L. Adamczyk, et al., Bulk Properties of the Medium Produced in Relativistic Heavy-Ion Collisions from the Beam Energy Scan Program, Phys. Rev. C96 (4) (2017) 044904. arXiv:1701.07065, doi:10.1103/PhysRevC.96.044904.
- [56] J. Adam, et al., Strange hadron production in Au+Au collisions at $\sqrt{s_{NN}} = 7.7, 11.5, 19.6, 27,$ and 39 GeV, Phys. Rev. C 102 (3) (2020) 034909. arXiv:1906.03732, doi:10.1103/PhysRevC.102.034909.
- [57] L. Ahle, et al., Excitation function of K+ and pi+ production in Au + Au reactions at 2/A-GeV to 10/A-GeV, Phys. Lett. B476 (2000) 1–8. arXiv:nucl-ex/9910008, doi:10.1016/S0370-2693(00)00037-X.
- [58] L. Ahle, et al., An Excitation function of K- and K+ production in Au + Au reactions at the AGS, Phys. Lett. B490 (2000) 53–60. arXiv:nucl-ex/0008010, doi:10.1016/S0370-2693(00)00916-3.
- [59] J. L. Klay, et al., Charged pion production in 2 to 8 agev central au+au collisions, Phys. Rev. C68 (2003) 054905. arXiv:nucl-ex/0306033, doi:10.1103/PhysRevC.68.054905.
- [60] J. L. Klay, et al., Longitudinal flow from 2-A-GeV to 8-A-GeV Au+Au collisions at the Brookhaven AGS, Phys. Rev. Lett. 88 (2002) 102301. arXiv:nucl-ex/0111006, doi:10.1103/PhysRevLett.88.102301.
- [61] B. B. Back, et al., Anti-lambda production in Au+Au collisions at 11.7-A-GeV/c, Phys. Rev. Lett. 87 (2001) 242301. arXiv:nucl-ex/0101008, doi:10.1103/PhysRevLett.87.242301.
- [62] C. Blume, C. Markert, Strange hadron production in heavy ion collisions from SPS to RHIC, Prog. Part. Nucl. Phys. 66 (2011) 834–879. arXiv:1105.2798, doi:10.1016/j.ppnp.2011.05.001.
- [63] B. B. Back, et al., Baryon rapidity loss in relativistic Au+Au collisions, Phys. Rev. Lett. 86 (2001) 1970–1973. arXiv:nucl-ex/0003007, doi:10.1103/PhysRevLett.86.1970.
- [64] J. Barrette, et al., Proton and pion production in Au + Au collisions at 10.8A-GeV/c, Phys. Rev. C62 (2000) 024901. arXiv:nucl-ex/9910004, doi:10.1103/PhysRevC.62.024901.
- [65] B. B. Back, et al., Production of phi mesons in Au+Au collisions at 11.7-A-GeV/c, Phys. Rev. C69 (2004) 054901. arXiv:nucl-ex/0304017, doi:10.1103/PhysRevC.69.054901.
- [66] P. Alba, W. Alberico, R. Bellwied, M. Bluhm, V. Mantovani Sarti, M. Nahrgang, C. Ratti, Freeze-out conditions from net-proton and net-charge fluctuations at RHIC, Phys. Lett. B738 (2014) 305–310. arXiv:1403.4903, doi:10.1016/j.physletb.2014.09.052.
- [67] D. Biswas, Formation of light nuclei at chemical freezeout: Description within a statistical thermal model, Phys. Rev. C 102 (2020) 054902. arXiv:2007.07680, doi:10.1103/PhysRevC.102.054902.
- [68] M. Tanabashi, et al., Review of Particle Physics, Phys. Rev. D98 (3) (2018) 030001. doi:10.1103/PhysRevD.98.030001.
- [69] S. Bhattacharyya, D. Biswas, S. K. Ghosh, R. Ray, P. Singha, Novel scheme for parametrizing the chemical freeze-out surface in Heavy Ion Collision Experiments, Phys. Rev. D 100 (5) (2019) 054037. arXiv:1904.00959, doi:10.

- 1103/PhysRevD.100.054037.
- [70] D. Biswas, Centrality dependence of chemical freeze-out parameters and strangeness equilibration in RHIC and LHC energies, *Adv. High Energy Phys.* 2021 (2021) 6611394. [arXiv:2003.10425](#), [doi:10.1155/2021/6611394](#).
- [71] S. Wheaton, J. Cleymans, M. Hauer, THERMUS: A Thermal model package for ROOT, *Comput. Phys. Commun.* 180 (2009) 84–106. [arXiv:hep-ph/0407174](#), [doi:10.1016/j.cpc.2008.08.001](#).
- [72] J. Cleymans, H. Oeschler, K. Redlich, S. Wheaton, Transition from baryonic to mesonic freeze-out, *Phys. Lett. B* 615 (2005) 50–54. [arXiv:hep-ph/0411187](#), [doi:10.1016/j.physletb.2005.03.074](#).
- [73] P. Huovinen, P. Petreczky, Hadron resonance gas with repulsive interactions, *J. Phys. Conf. Ser.* 1070 (1) (2018) 012004. [doi:10.1088/1742-6596/1070/1/012004](#).
- [74] S. Chatterjee, S. Das, L. Kumar, D. Mishra, B. Mohanty, R. Sahoo, N. Sharma, Freeze-Out Parameters in Heavy-Ion Collisions at AGS, SPS, RHIC, and LHC Energies, *Adv. High Energy Phys.* 2015 (2015) 349013. [doi:10.1155/2015/349013](#).
- [75] M. Abdallah, et al., Cumulants and correlation functions of net-proton, proton, and antiproton multiplicity distributions in Au+Au collisions at energies available at the BNL Relativistic Heavy Ion Collider, *Phys. Rev. C* 104 (2) (2021) 024902. [arXiv:2101.12413](#), [doi:10.1103/PhysRevC.104.024902](#).
- [76] J. Adam, et al., Enhanced production of multi-strange hadrons in high-multiplicity proton-proton collisions, *Nature Phys.* 13 (2017) 535–539. [arXiv:1606.07424](#), [doi:10.1038/nphys4111](#).
- [77] M. Gazdzicki, M. I. Gorenstein, On the early stage of nucleus-nucleus collisions, *Acta Phys. Polon. B* 30 (1999) 2705. [arXiv:hep-ph/9803462](#).
- [78] M. Gazdzicki, Energy scan program at the CERN SPS and an observation of the deconfinement phase transition in nucleus nucleus collisions, *J. Phys. G* 30 (2004) S161–S168. [arXiv:hep-ph/0305176](#), [doi:10.1088/0954-3899/30/1/015](#).
- [79] E. L. Bratkovskaya, M. Bleicher, M. Reiter, S. Soff, H. Stoecker, M. van Leeuwen, S. A. Bass, W. Cassing, Strangeness dynamics and transverse pressure in relativistic nucleus-nucleus collisions, *Phys. Rev. C* 69 (2004) 054907. [arXiv:nucl-th/0402026](#), [doi:10.1103/PhysRevC.69.054907](#).
- [80] V. Koch, A. Majumder, J. Randrup, Signals of spinodal hadronization: Strangeness trapping, *Phys. Rev. C* 72 (2005) 064903. [arXiv:nucl-th/0509030](#), [doi:10.1103/PhysRevC.72.064903](#).
- [81] J. K. Nayak, S. Banik, J.-e. Alam, The horn in the kaon to pion ratio, *Phys. Rev. C* 82 (2010) 024914. [arXiv:1006.2972](#), [doi:10.1103/PhysRevC.82.024914](#).
- [82] C. Li, D. Biswas, N. R. Sahoo, Cumulants of net-strangeness multiplicity distributions at energies available at the BNL Relativistic Heavy Ion Collider, *Phys. Rev. C* 107 (6) (2023) 064905. [arXiv:2209.10343](#), [doi:10.1103/PhysRevC.107.064905](#).
- [83] J. Adam, et al., Nonmonotonic Energy Dependence of Net-Proton Number Fluctuations, *Phys. Rev. Lett.* 126 (9) (2021) 092301. [arXiv:2001.02852](#), [doi:10.1103/PhysRevLett.126.092301](#).
- [84] P. Garg, D. K. Mishra, P. K. Netrakanti, B. Mohanty, A. K. Mohanty, B. K. Singh, N. Xu, Conserved number fluctuations in a hadron resonance gas model, *Phys. Lett. B* 726 (2013) 691–696. [arXiv:1304.7133](#), [doi:10.1016/j.physletb.2013.09.019](#).
- [85] D. K. Mishra, P. Garg, P. K. Netrakanti, A. K. Mohanty, Effect of resonance decay on conserved number fluctuations in a hadron resonance gas model, *Phys. Rev. C* 94 (1) (2016) 014905. [arXiv:1607.01875](#), [doi:10.1103/PhysRevC.94.014905](#).
- [86] S. Pal, G. Kadam, A. Bhattacharyya, Hadron resonance gas model with repulsive mean-field interactions: Specific heat, isothermal compressibility and speed of sound, *Nucl. Phys. A* 1023 (2022) 122464. [arXiv:2104.08531](#), [doi:10.1016/j.nuclphysa.2022.122464](#).